



# Biomechanical comparison of spinal cord compression types occurring in Degenerative Cervical Myelopathy

Simon Lévy, Guillaume Baucher, Pierre-Hugues Roche, Morgane Evin,  
Virginie Callot, Pierre-Jean Arnoux

## ► To cite this version:

Simon Lévy, Guillaume Baucher, Pierre-Hugues Roche, Morgane Evin, Virginie Callot, et al.. Biomechanical comparison of spinal cord compression types occurring in Degenerative Cervical Myelopathy. Clinical Biomechanics, 2020, pp.105174. 10.1016/j.clinbiomech.2020.105174 . hal-02992367

**HAL Id: hal-02992367**

**<https://amu.hal.science/hal-02992367>**

Submitted on 9 Dec 2020

**HAL** is a multi-disciplinary open access archive for the deposit and dissemination of scientific research documents, whether they are published or not. The documents may come from teaching and research institutions in France or abroad, or from public or private research centers.

L'archive ouverte pluridisciplinaire **HAL**, est destinée au dépôt et à la diffusion de documents scientifiques de niveau recherche, publiés ou non, émanant des établissements d'enseignement et de recherche français ou étrangers, des laboratoires publics ou privés.

# **Biomechanical comparison of spinal cord compression types occurring in Degenerative Cervical Myelopathy**

Simon Lévy<sup>1-4</sup>, Guillaume Baucher<sup>4,5</sup>, Pierre-Hugues Roche<sup>4,5</sup>, Morgane Evin<sup>3,4</sup>, Virginie  
Callot<sup>1,2,4</sup>, Pierre-Jean Arnoux<sup>3,4</sup>

## **Affiliations**

<sup>1</sup> Aix-Marseille Univ, CNRS, CRMBM, Marseille, France

<sup>2</sup> APHM, Hopital Universitaire Timone, CEMEREM, Marseille, France

<sup>3</sup> Aix-Marseille Univ, IFSTTAR, LBA, Marseille, France

<sup>4</sup> iLab-Spine International Associated Laboratory, Marseille-Montreal, France-Canada

<sup>5</sup> APHM, Hopital Nord, Neurosurgery Department, Marseille, France

## **Corresponding author**

Pierre-Jean Arnoux

LBA, Faculté de Médecine Nord, Aix-Marseille Université

Bd Pierre Dramard

13916 Marseille cedex 20, France

Office: +334 91 65 80 06 | Email: [pierre-jean.arnoux@ifsttar.fr](mailto:pierre-jean.arnoux@ifsttar.fr)

# Abstract

**Objective:** To study spinal cord compressions occurring in Degenerative Cervical Myelopathy (DCM) using a comprehensive biomechanical model defined by actual features observed in patients, in a view to better understand the pathogenesis and further predict patients evolution.

**Methods:** Anatomical MRIs from 20 DCM patients were collected. Compression indices derived from spinal canal and spinal cord were measured at the compression site. Mean values were compared to values reported in literature and to the *Spine Model for Safety and Surgery* (comprehensive 3D finite element model of the spine), further used for simulations. Based on those results, a 30% reduction in cord cross-sectional area at C5-C6 intervertebral disk was defined as the compression threshold inducing myelopathy. Four main compression patterns were simulated. Median diffuse, median focal and lateral compression types were modelled as a migration of the disk into the spinal canal evenly, at the central line only and laterally, respectively. Circumferential type involved a posterior compression by the ligamentum flavum. All constraints in spinal cord were quantified along inferior-superior axis, along compression development and within atlas-defined spinal cord regions.

**Results:** Regardless of compression types, predominant stress was found along anteroposterior axis but also along inferior-superior axis, attributable to a slight sliding of the disk in that direction because of natural spine anatomical restrictions. Anterior GM and WM regions globally received the highest stress while lateral pathways were the least affected. Compression applied along the complete anterior side of the cord (median diffuse) globally induced the highest constraints. Additional posterior compression by ligamentum flavum (circumferential) might focus constraints in the anterior gray matter region. Along inferior-superior axis, median diffuse and circumferential types showed a peak of constraints at compression site while median focal and lateral types showed lower constraints values but extending further.

**Conclusion:** Median diffuse type would be the most detrimental based on stress amplitude. Anterior regions would be the most at risk, except for circumferential type where posterior regions would be equally affected. Ischemia would be a significant component in addition to applying constraints to explain the pathogenesis of DCM, in particular for lateral pathways. Future work will look at patient-specific simulations and

1 relation with clinical symptoms. Biomechanical models could become strong predictors  
2 of degenerative changes.

3

4 **Keywords:** spinal cord, spinal cord compression, biomechanical simulations,  
5 degenerative cervical myelopathy, finite element modelling

# 1. Introduction

Degenerative Cervical Myelopathy (DCM) is the most common progressive non-traumatic disorder of the spinal cord (SC) in elderly population with a prevalence of 605 per million people in North America (1). Eighty-seven percent of global population above 60 years old is estimated to present one or more severely degenerated cervical levels (2). DCM results from degenerative changes of the cervical spine with aging causing spinal canal stenosis, cord compression and eventually myelopathy (i.e. SC-related neurologic deficit). Degenerative changes are multiple and can happen concurrently or individually (1). On the anterior side of the cord, intervertebral disk draining causing disk material migration into the spinal canal, spondylitis with osteophytes development along with hypertrophy of the posterior longitudinal ligament (PLL) progressively reduce the spinal canal cross section. On the opposite side, the spinal canal is reduced by hypertrophy of the ligamentum flavum. Compression is suspected to first disrupt tissue perfusion and metabolism, which then leads to expanding tissue necrosis (cell loss, axonal demyelination, Wallerian degeneration) (3–5). In addition to the chronic static cord compression, everyday life neck motion (flexion, extension) is expected to add repeated traumas to the cord (dynamic effects). However, the respective role of each process in tissue degeneration yielding myelopathy remains unknown. The multiple processes aforementioned induce a high variability in the patients' clinical presentation and the compression patterns observed on MRI or CT scans. Severity of symptoms is therefore hardly predictable.

The SC compression process is intrinsically mechanical. Finite element models are therefore very well suited to study SC compression processes occurring in DCM degeneration. Several biomechanical studies already proposed DCM compression models. Nishida et al (6) first studied the contribution of static and dynamic anterior compressions of the cord for three different patterns (central, lateral, diffuse). Kim et al (7) investigated the individual effects of different patterns of ossification of the PLL and ligamentum flavum. Nishida et al then explored the static and dynamic effects of the ossification of the PLL (8). Finally, Khuyagbaatar et al (9) modelled both single-level and multi-level compressions caused by ossification of the PLL.

In all of these studies, the different processes involved were not simulated concurrently. Resulting stresses were only analyzed based on visual assessment of the stress maps or by quantification at a specific compression stage and level without

1 comparison across spinal pathways, compression development or inferior-superior (I-S)  
2 axis. Moreover, models were often simplified with unnatural compression loading, which  
3 is useful to identify the specific effects of a given process but could miss some important  
4 features induced by the natural human anatomy.

5 In this work, simulations of the main compression patterns derived from clinical  
6 MR exploration of 20 DCM patients were designed using a detailed and comprehensive  
7 cervical SC model. Quantitative compression features measurements from MRI data and  
8 derived from literature were integrated. All resulting constraints were analyzed along the  
9 I-S axis, along compression development and across atlas-defined SC regions so as to  
10 identify the specificity of each compression pattern. Such analysis can help understand  
11 the multiple degenerative processes associated with DCM and identify the most  
12 detrimental pattern. Those simulations could guide clinicians in the treatment, surgical  
13 planning and/or prognosis of this pathology.

## 2. Material and Methods

### 2.1. Compression features from literature review

#### 2.1.1. Most frequently affected level

Intervertebral disk level C5-C6 is the most frequently compressed level in DCM patients (10,11). It is hypothesized to be due to the higher mobility of that segment compared to others (12). It is also among the two segments with smallest anteroposterior (A-P) spinal canal diameter (13).

#### 2.1.2. Compression threshold inducing tissue degeneration

In literature, SC compression has been quantified using different morphological measurements (Table 1).

First studies chose to measure the spinal canal A-P diameter. Arnold et al. (14) shows a strong involvement of age and of this measure at C5 in myelopathy severity. According to Fehlings et al. (4) based on such data, a diameter of less than 12 mm would be a critical threshold in the development of DCM, while a normal cervical spinal canal diameter would be around 17-18 mm (15,16). In close agreement, Adams and Logue (17) found an average A-P spinal canal diameter of 11.8 mm in their DCM-only group, while the average diameter without osteophyte was 17.2 mm and the average diameter in the control group was 19.2 mm. Those values are also in agreement with Edwards and LaRocca' study (11) on narrow cervical spinal canal but they slightly differ from the values reported in Burrows et al. (15) with a median sagittal canal diameter of 14.5 mm at C5 in degenerative cervical spondylosis. Ogino et al. (13) also measured a larger critical canal diameter with around 13 mm for the DCM group with respect to around 16 mm for the control group at C5.

The Maximum Canal Compromise (MCC) and Maximum SC Compression (MSCC) indices were also proposed to predict patients' surgical outcome (18–22). MCC (resp. MSCC) were calculated as  $100 \times \left(1 - \frac{d_i}{(d_a + d_b)/2}\right) \%$  with  $d_i$ ,  $d_a$  and  $d_b$  being the A-P canal (resp. cord) diameters at compression level, at the nearest normal level above and below compression level respectively. In DCM patients prior to surgery, reported MCC mean values were 35.3% (N=71)(18) and 49.2% (N=114)(21); reported MSCC values were 27.4% (N=71)(18), 33.9% (N=114)(21) and 31.5% (N=113)(23). However, the calculation of those indices might be prone to substantial rater bias related to the

definition of the nearest normal levels above and below compression level, largely depending on the number of compressed levels in the patient.

Compression assessment based on the SC Cross-Sectional Area (CSA) might be less prone to bias and more directly related to the compression-induced tissue damage. According to Penning et al.' study (24), the critical SC compression threshold inducing myelopathy is a CSA of  $\sim 60 \text{ mm}^2$  measured in CT myelography at C5-C6 vertebral level, corresponding to a 30% reduction in CSA compared to controls. Note that this threshold is in agreement with the reported MSCC values on DCM. In their cohort of 113 DCM patients in need of decompression surgery, Li et al. reported a mean CSA and MSCC of  $51.15 \text{ mm}^2$  and 31.5% respectively (23).

Finally, the A-P compression ratio has also been employed. It is the ratio of the A-P diameter of the cord over its right-left (R-L) diameter (Figure 1). Li et al. measured a mean ratio of 34.25% across the same cohort (23). However, this index was unsuccessfully correlated to decompression surgery outcome.

## **2.2. Compression features from acquired MRI data**

To complete and balance the data heterogeneity in literature regarding DCM features, anatomical MR images of 20 diagnosed DCM adult patients acquired at 3T (Magnetom Verio, Siemens Healthcare) at CEMEREM (La Timone Hospital, APHM, Marseille, France) were retrospectively examined.

### *2.2.1. Most frequently affected level*

C4-C5 and C5-C6 were the most frequent compression levels (N=8 respectively) in the cohort.

### *2.2.2. Compression threshold inducing tissue degeneration*

The morphological features of DCM compressions were inspected on T2\*-weighted and T1-weighted images. The following measurements were performed on T1-weighted images at the maximum compression level: A-P and R-L spinal canal diameters, A-P and R-L cord diameters (used to calculate A-P cord compression), spinal canal and cord Cross-Sectional Area (CSA), cord A-P occupation (cord A-P diameter/canal A-P diameter) and cord CSA occupation (cord CSA/canal CSA). Those indices are defined on Figure 1. Measurements were performed manually using *Horos* (horosproject.org).



### 2.2.3. Elected compression features for simulations

Considering morphometric indices based on SC more directly related to the constraint applying in it, and given the proximity between measurements derived from MRI data and literature (see Table 1 and Results section), the SC CSA was elected to define the compression threshold. A SC CSA of 70% with respect to the initial CSA (equivalent to a 30% CSA reduction) was defined as threshold inducing myelopathy at C5-C6 intervertebral disk level.

### 2.2.4. Observed compression types

Anatomical MRI images showed various compression patterns which were classified into 4 main types (Figure 2) in agreement with previous studies (6,25,26): median and diffuse (N=9), median and focal (N=2), lateral (N=5), circumferential (N=4). Note that paramedian focal compressions (compression point not exactly in the median sagittal plan of the cord, as shown in the MRI scan for median focal type in Figure 2) would be included in median focal type.

## 2.3. Simulations

### 2.3.1. Finite element model description

The *Spine Model for Safety and Surgery* (27,28) was employed to simulate each type of SC compression. This is a 3D finite element model of the spine made out of the CT scan of a 32-year old healthy male human subject. It includes vertebrae, ligaments, intervertebral disks, SC gray and white matter (GM, WM), spinal roots, dura and pia matter, dentate ligaments and ganglion. GM and WM were modelled according to an elastic law with tangent moduli of  $1.67 \times 10^{-1}$  and  $0.9 \times 10^{-1}$  MPa respectively (29). Their geometry was defined based on a high-resolution MRI atlas (30). Anterior and posterior GM regions as well as WM dorsal column, WM lateral motor, WM lateral sensory and WM anterior spinal pathway regions were defined according to histological and MRI atlases (31,32). SC sub-regions were modelled as a continuous mesh. SC was meshed with tetrahedral elements, as were the Intervertebral Disk (IVD), made of a nucleus and an annulus (28). The complete description of the model parameters used can be found in Table 2. For clarity purposes, in the subsequent text, the posterior > anterior axis was defined along  $\vec{x}$ , the right > left axis along  $\vec{y}$  and the inferior > superior axis along  $\vec{z}$  (see Figure 2).

1 Since literature review and MRI data both showed that C5-C6 was the most  
2 frequently affected level in DCM and since this study focused on single-level  
3 compression, the cervical segment from C4 to C6 was extracted. It also enabled to remain  
4 within acceptable simulation times and manageable memory size.

### 5 *2.3.2. General simulation features*

6 Simulations were designed with HyperMesh v17 and performed with RADIOSS v17  
7 (Altair Engineering Inc., MI, USA).

8 C4 and C6 vertebrae were fixed. C5-C6 IVD and C5-C6 ligamentum flavum were  
9 used to impose the SC loading with a given kinematic condition (see below). Constraints  
10 on those entities were therefore not considered. To account for the quasi-static behavior  
11 of the degenerative process, the kinetic energy relaxation was forced at each computing  
12 step.

### 13 *2.3.3. Diffuse median compression*

14 All nodes of C5-C6 IVD were translated along  $-\vec{x}$  about 9.9mm so as to reach a 70%  
15 compression ratio in CSA at the compression site.

### 16 *2.3.4. Acute median compression*

17 C5-C6 IVD was divided into two groups of nodes. The central line (~6.5mm  
18 thickness out of 20mm diameter) was translated by 9.8mm along  $-\vec{x}$  while the remaining  
19 nodes were translated by 7.9mm so as to reach a compression ratio of 70% and avoid  
20 rupture of too many elements.

### 21 *2.3.5. Asymmetric compression*

22 C5-C6 IVD was divided into four groups of nodes. The most left part of the disk  
23 (7.4mm thick), a central-left line (2.5mm thick), the central line (1.9mm thick) and the  
24 remaining right part of the disk (7.6mm thick) were translated along  $-\vec{x}$  by 11.2mm,  
25 10.5mm, 8.5mm and 8.1mm respectively. Such design enabled us to create asymmetry in  
26 the compression while still reaching a 70% compression ratio.

### 27 *2.3.6. Circumferential compression*

28 All nodes of C5-C6 IVD were translated along  $-\vec{x}$  by 4.4mm while all nodes of C5-  
29 C6 ligamentum flavum were translated along  $+\vec{x}$  by 4.4mm.

## 2.4. Quantification

Stresses along X, Y, Z, shear stresses in XY, YZ, ZX and Von Mises stress were extracted with HyperView v2017 and Compose v2019.2 (Altair Engineering Inc., MI, USA). Data were processed with Python v3.6.

### *2.4.1. Study along inferior-superior axis*

To mitigate outliers effect, the 95<sup>th</sup> percentile of each constraint absolute value within SC at each millimeter was extracted for each compression type and plotted along the I-S axis. The absolute value enabled to be independent from the axes direction definition.

### *2.4.2. Study across compression development course*

For each simulation step, the 95<sup>th</sup> percentile of each constraint absolute value within the whole SC was extracted for each compression type.

### *2.4.3. Study across spinal cord regions*

The 95<sup>th</sup> percentile of each constraint absolute value within each of the 6 SC regions (anterior and posterior GM, WM dorsal column, WM lateral motor, WM lateral sensory and WM anterior pathways) was extracted for each compression type and pictured on a transversal unwrapped SC map. Note that left and right regions were quantified together to get rid of bias caused by potential asymmetry in compression types (e.g., lateral type).

### 3. Results

Mean spinal canal and cord measurements across patients performed on MRI data were compared to literature data in Table 1. Those measurements were normalized to initial SM2S model dimensions (1<sup>st</sup> row) to determine the equivalent compression in the model. Compression indices based on spinal canal dimensions showed poor agreement between our DCM cohort, SM2S model and literature data available. However, cord-based indices, and in particular, MSCC, A-P cord diameter and cord CSA showed a rough agreement around a 30% compression value between the measurements performed on the DCM cohort with respect to initial SM2S dimensions and literature data with respect to controls (equivalent to an index value of 70% with respect to the uncompressed state).

The similarity obtained between the designed simulations and the observed DCM compression patterns on transversal MRIs can be observed on Figure 2. The median diffuse compression is mainly caused by the migration of a large portion of the disk into the canal in addition to osteophyte development. The SC is pushed from its anterior side to the posterior side of the canal. In the median focal type, the compression is more local, predominantly caused by osteophyte developments or herniated disk, which was modelled by a more prominent migration of the central A-P line of the disk. The lateral compression is caused by an asymmetric degeneration of the disk and/or osteophyte development; it was simulated by a more prominent migration of the left side of the disk. Finally, the circumferential compression type involves an additional process: hypertrophy and bulking of the ligament flavum induce a posterior stenosis of the spinal canal while disk migration and/or osteophyte development constrict the cord anteriorly.

A sole observation of constraint maps (as in Figure 2) does not enable to detect differences between compression types. For all types, GM appears as the structure with the most constraints, which is attributable to its highest rigidity compared to WM. Profiles along I-S axis look similar and so far, history of the compression development process is missing.

The quantitative constraints profile along the I-S axis in the whole SC is presented in Figure 3 for each compression type. Two profiles can be identified. Median diffuse and circumferential types show a peak of the constraints at the level of compression whereas median focal and lateral types show low constraint values but extending over a larger height of the SC, spreading from upper C5 level down to lower C6. Such features would not have been detectable with a sole qualitative observation of the constraints maps

(Figure 2), hence the value of the quantitative analysis. Median diffuse appears as the compression type inducing the highest constraint to the SC tissue with a peak of the Von Mises stress at 0.15MPa and of  $\sigma_X$  (stress along  $\vec{x}$ ) at 0.14MPa. For all types, the highest directional stress is along X while the highest shear stress is in the ZX plane.

Figure 4 presents the evolution of constraints within cord along the development of the pathology until compression threshold is reached. A linear rise of the constraints can be observed with the development of the compression but at different pace according to compression types. Constraints in SC start to increase earlier for median focal and lateral types but at a slower pace than other types. Median diffuse show the latest rise of the constraints and the fastest pace. Nevertheless, care has to be taken when comparing those results as time scale and respective timings of individual degenerative changes are unknown and may highly vary across population. Again, for all types, the constraints are dominated by the stress along X and the shear stress in the ZX plane.

Figure 5 presents constraints analysis by SC sub-regions. Spinal pathways were affected differently according to compression type. Globally, highest constraint values were found for Von Mises and directional stresses. Shear stresses in XY and YZ planes showed the lowest contributions.

The median diffuse type induced the most damage, mainly in GM and WM anterior regions. Interestingly, this compression type also showed the highest shear stress value in ZX plane (for the GM posterior horns). This type also showed the highest stress along Z (within the anterior WM).

The median focal type also showed high  $\sigma_X$  in the central regions of the cord (anterior WM, GM and dorsal columns) but posterior GM horns were less affected than with the diffuse type.

The lateral compression type showed a similar profile as the median focal type but with lowest constraint values (Von Mises,  $\sigma_X$ ). Of note, although the compression pattern is asymmetric, the lateral pathways were not the most affected. Highest constraints were found in anterior regions.

Finally, the circumferential type almost showed no shear stress and constraints were mainly the stress along X and Von Mises stress. Interestingly, the stress along X was similarly distributed between anterior and posterior regions. Indeed, this compression pattern was the one with the highest  $\sigma_X$  in posterior GM horns and dorsal columns.

- 1
- 2
- 3

## 4. Discussion

In this work, biomechanical constraints applying in the SC during typical DCM compressions were studied and the effect of compression pattern was investigated. In a view to perform realistic simulations, compression features were defined based on MRI data and morphological studies available in literature. A compression threshold inducing myelopathy was defined based on the SC CSA and four compression patterns were simulated using a detailed and comprehensive finite element model of the spine. Differences in terms of I-S profile of the constraints at compression threshold, constraint evolution along development of degenerations and constraints distribution across SC sub-regions were examined.

### 4.1. Main findings

Regardless of the compression type, the main constraints standing out were along the A-P axis, as well as along I-S axis in anterior regions. In addition to the obvious A-P compression, the anatomy (alignment between the disk and the opposite vertebrae posterior part) might also induce a sliding of the disk in the I-S direction, resulting in constraints along this axis as well. Moreover, GM is globally the most affected structure, which is attributable to its higher rigidity compared to WM. This result is in agreement with histologic and clinicopathologic studies reporting most severely affected central GM, anterior cell loss and GM infarction in DCM patients (4,13). Also, interestingly, ischemia and compression are thought to be additive causes to tissue necrosis. Experimental studies in dogs demonstrated the combined effects of those two processes, with anterior SC compression and ligation of segmental arteries (33), and with cervical compression and obstruction of the arterial plexus (34). Ischemia clearly exacerbated the pathologic effects of compression and yielded a particular vulnerability of corticospinal tracts to injury. Such observation was substantiated by clinicopathologic studies reporting that corticospinal tracts demyelination was one of the first pathological changes in DCM (13). In light of those findings, our results suggest that lateral WM tracts damage occurring in DCM cannot be explained by applying constraints only, but that ischemia would be a necessary component to this process.

In agreement with previous biomechanical studies on DCM compressions (6,9), the median diffuse type induced the highest constraints. Median focal and lateral types differed especially regarding the constraints profile along the I-S axis, suggesting that SC

would need to be screened more carefully rostral and caudal to the compression site for such compression patterns. This result can be explained by the more local compression; the cord needs to be confined in a more restricted area, involving opposite forces applying above and below the compression site to clench the cord. The circumferential type, involving both anterior and posterior compression by hypertrophy of the ligamentum flavum, exhibited particular constraints distribution across SC sub-regions. Very low shear stresses were observed and constraints were mainly focused in the A-P axis. Effects of ligaments ossification on the stress distribution in SC have been studied at thoracic and cervical levels (7–9) but they have never been compared to other compression types with identical spine models. Quantification results may substantially differ across models. The current study enables to directly identify the specific effects of each type, and in particular, the circumferential type would be the one inducing the highest constraints along A-P axis in posterior GM horns.

Furthermore, this work investigated the evolution of stresses in SC as DCM degenerations develop. Such analysis could guide neurosurgeons in defining the critical time to prescribe surgery or in identifying the most detrimental degenerative changes. For instance, results obtained here would suggest that lateral and median focal types take more degenerative changes (displacement) or more time to set up and reach the threshold defined as inducing myelopathy. However, to translate those results to real life, timings of each degenerative process with respect to each other need to be known. But those degenerative processes and their timing are very likely to vary across patients. Simulations designed specifically on the patient morphology (patient-specific simulations) would therefore be required to predict the pathology evolution.

Beyond that, this study proposes an exhaustive quantitative analysis of the constraints at different scales (across degeneration process, I-S axis, SC regions) which, to the best of our knowledge, has been rarely done in the literature, probably because of the large memory size and lack of tools available for such study. However, such analysis is crucial to explore and understand the tissue degeneration processes of this pathology.

## **4.2. Limitations and perspectives**

Compressions occurring in DCM patients are highly variable, as are the symptoms. For the study purposes, compression patterns were classified into 4 main types. Interestingly, this classification was found to be consistent across the literature (6,9). However, real cases often mix those types either at different intervertebral levels or even



1 at a single level. Designing such compression patterns would come to patient-specific  
2 simulations, relevant for report case studies.

3 The same compression threshold was defined for each type. However, given the  
4 variability of constraints distribution, this threshold is likely to differ across types. No  
5 data available in the literature enabled to provide an answer to this question. Further  
6 investigations, in association with MRI examinations and patient-specific simulations,  
7 will look at the definition of this threshold based on the actual constraints value applying  
8 in the tissue, which might be a more direct surrogate than the CSA. Anyhow, indices  
9 based on spinal canal dimensions appeared less reliable to define the myelopathy or  
10 symptomatic threshold than indices based on SC dimensions because of a larger  
11 variability.

12 In the current study, only static effects of compression were considered. Dynamic  
13 effects (with repeated neck flexion and extension) are suspected to have a significant  
14 impact on myelopathy development too. In a simplified model of the cervical spine, they  
15 were shown to have a different effect on stress distribution in the cord (6) but this effect  
16 was not quantified. Integration of such effects in the current model would be relevant.

17 Results suggest that the choice of tissue rigidity for GM with regards to WM have a  
18 strong impact on the resulting stress values in those two structures. Even though limited  
19 literature exists on this topic for human, three studies (two groups) agreed on a higher  
20 stiffness of GM compared to WM, in bovine cervical cord by tensile testing (29,35) and  
21 in mice SC using atomic force microscopic indentation and tensile measurements (36).  
22 One study found no significant difference using pipette aspiration method in rabbit SC  
23 (37). In this study, values reported for bovine cervical cord were used with higher  
24 stiffness of GM (29). Although it is likely to observe the same behavior in humans,  
25 everything has still to be shown. Therefore, stress values reported here can only be  
26 considered relatively. In addition, if GM turned out to be less rigid than WM in humans,  
27 results of these simulations might be challenged.

28 Furthermore, Koser et al. (36) reported significant difference in compression  
29 measurements depending on tissue orientations, for both WM and GM. They even found  
30 significant differences across GM regions, with the dorsal horn being stiffer than the  
31 ventral horn, while WM would be transversely isotropic. Obtaining similar data for  
32 human SC would refine the model and provide more insights for regional analysis.

33 The acknowledged hypothesis is that the main components in DCM pathogenesis are  
34 tissue compression and ischemia, with the two processes working both sequentially

(cervical compression inducing arterial obstruction causing ischemia) and additively (ischemia exacerbating compression pathological effects) (4). For this reason, the study focused on mechanical stresses and strain measurement were not included. Including strain in such an analysis could bring more insights in the understanding of the pathology, but this would require a more complex and accurate modelling than the elastic law used here, with failure criteria. Unfortunately, such data are not available yet.

Impacts on tissue perfusion were not modelled in this study either. SC vascular network is very complex and may vary across individuals. Moreover, the characterization of its effect on the tissue mechanical properties is challenging. However, as described earlier with regards to corticospinal tracts early demyelination, ischemia effects are a key component in the pathogenesis of DCM. Ashareef et al. (38) implemented a simple model of the anterior spinal artery and five of its branches to investigate how differently anterior, posterior and anteroposterior compression would affect blood supply. One of their main findings was that the perfusion disruption caused by the compression of the main arteries could potentially be compensated by an increased blood flow in non-compressed arteries. However, effects of and on capillary network within tissue was not investigated. This field of research still remains unexplored but would help refine the model.

The time scale of degenerative changes leading to cord compression remains unknown but clearly extends over several years and even decades. During this period of time, as tissue gets more and more compressed, tissue degeneration also induces a change in tissue properties. In this study, this change during development of the compression was not taken into account and tissue properties were fixed during the entire length of the simulations. We expect that it would only affect the constraints values but not the overall trends and distributions observed. Regarding quantification more particularly, the 95<sup>th</sup> percentile of the absolute constraints value was preferred over the maximum value here to mitigate outliers' effect but this index can yield slightly different values depending on the considered regions. No gold standard has been agreed upon so far and studies rarely mention the metric used.

Furthermore, only three vertebral levels were considered which limits the SC extent along the I-S axis under investigation. Moreover, the compression consequently occurs at unequal length from top and bottom of the model, which were fixed. A choice was also made to leave the whole middle vertebral level (C5) free, neglecting potential constraints from surrounding muscles. On the one hand, performing the same compression

1 simulations on a longer I-S extent of the model might let higher degrees of freedom to the  
2 cord and increase the time necessary to reach compression threshold. On the other hand,  
3 fixing intermediate vertebrae (or including neck muscles in the model) would reduce SC  
4 mobility and help reach the compression threshold faster.

## 5. Conclusion

Integrating representative morphologic measurements of DCM compressions into a comprehensive spine model and by means of an exhaustive quantitative analysis of the constraints, different compression patterns were shown to induce different constraint profiles along the I-S axis, along degenerative process development and across SC regions. Median diffuse compression was found to be the most detrimental pattern, causing the highest constraints with the fastest pace. Anterior GM and WM pathways would be the most affected regions, except for circumferential compression where posterior GM and dorsal columns would be equally at stake. In contrast, lateral WM pathways demyelination observed in DCM would not be attributable to applying constraints only, but to the combined effects of compression and ischemia.

Future work will look at patient-specific simulations in association with microstructural assessment of the tissue by MRI in a view to define a threshold inducing myelopathy based on actual applying constraints. In the near future, for patients showing stenosis at the preclinical stage, reliable simulation models could be strong predictors of potential deficits and could help prompt preventive surgery. Such an approach is in stark contrast with the current policy as consensus still is to indicate decompression at the time of clinical impairment without any guarantee for recovery.

## 6. Table and figure captions

	A-P canal diameter (mm)	R-L canal diameter (mm)	A-P cord diameter (mm)	R-L cord diameter (mm)	A-P/R-L cord ratio (%)	Canal CSA (mm <sup>2</sup> )	Cord CSA (mm <sup>2</sup> )	Cord A-P occupation (%)	Cord CSA occupation (%)
SM2S model at C5-C6 (no compression)	13.7	20.4	7.7	13.7	56.3	214.1	87.1	56.2	40.7
Mean at compression	7	16.2	5.7	12.3	47.1	93.6	58.3	81.8	62.3
SD across patients	1.1	2.5	1.1	1.9	9.8	23.3	16.4	7.8	10.3
Equivalent compression compared to SM2S (2 <sup>nd</sup> row/1 <sup>st</sup> row)	50.8 %	79.1 %	74.3 %	90.2 %	83.6 %	43.7 %	67 %	145.6 %	153.1 %
Literature (% control value when available or native unit)									
(Adams and Logue, 1971), N=18, at max comp.	64.8%								
(Edwards and LaRocca, 1983), N=63, at C5-C6	12.7 mm								
(Burrows, 1963), N=24, at C5	87.9%								
(Arnold, 1955), N=100, at C5	14 mm								
(Ogino et al., 1983), N=90, at C5	88.8%								
(Penning et al., 1986), N=80, at C5-C6							70%		
(Li et al., 2018), N=113, at max comp.					34.25		51.15		

A-P: anteroposterior; R-L: Right-Left; CSA: Cross-Sectional Area; SD: standard deviation; N: DCM patients sample size; at max. comp: at level of maximal compression.

**Table 1.** Compression indices compared between SM2S model at t=0 (row 1, dark gray background), DCM patients group (rows 2, 3) and literature (row 5 and below). Row 4 reports the equivalent percentage compression of SM2S model if the mean compression measured in patients is applied to the model. The compression indices found in literature were reported in percentage with regards to controls when data were available (italic format within table). For easier visualization, background of spinal canal-based indices was colored in light gray. Agreement of cord-based indices around a value of 70% compression (with regards to uncompressed value) was highlighted in green. Compression indices are defined in Figure 1.

Anatomical entity	Element type	Number of integration point	Characteristic length (mm)	Material law	Material property	Reference
Gray matter	Tetrahedral	4	0.41 – 0.79	Linear elastic	$\rho = 0.001$ $\nu = 0.4$ $E = 0.167$	(Ichihara et al., 2001)
White matter	Tetrahedral	4	0.39 – 0.83	Linear elastic	$\rho = 0.001$ $\nu = 0.4$ $E = 0.09$	(Ichihara et al., 2001)
Pia mater	Shell	3	0.76 – 0.78	Linear elastic	$\rho = 0.001$ $\nu = 0.45$ $E = 2.3$	(Fradet et al., 2016)
Dura mater	Shell	3	0.74 – 0.89	Linear elastic	$\rho = 0.001$ $\nu = 0.45$ $E = 5.0$	(Fradet et al., 2016)
Spinal roots	Spring	2	4 – 10		$M = 0.1$ $K = 0.133$	(Kulkarni et al., 2007)
Dentate ligaments	Shell	3	0.48 – 0.55	Linear elastic	$\rho = 0.001$ $\nu = 0.4$ $E = 10.0$	(Fradet et al., 2016)
Intervertebral disk						(Lee et al., 2000; Schmidt et al., 2007)
Annulus	Hexahedral	8	0.69 – 1.39	Ogden, Mooney-Rivlin	$\rho = 0.0012$ $\nu = 0.45$ $\mu_1 = 0.47$ $\mu_2 = -0.118$ $\alpha_1 = 2.0$ $\alpha_2 = -2.0$	
Nucleus	Hexahedral	8	0.73 – 1.21	Ogden, Mooney-Rivlin	$\rho = 0.001$ $\nu = 0.495$ $\mu_1 = 1.27$	

**Table 2.** Model parameters used for simulations.  $\rho$ : density (g.mm-3),  $E$ : Young's Modulus (MPa),  $\nu$ : Poisson's ratio,  $M$ : mass (g),  $K$ : stiffness (N),  $E_t$ : tangent modulus (MPa), ( $\mu_1$ ,  $\mu_2$ ): ground shear hyperelastic modulus (MPa), ( $\alpha_1$ ,  $\alpha_2$ ): material exponent parameters (MPa).

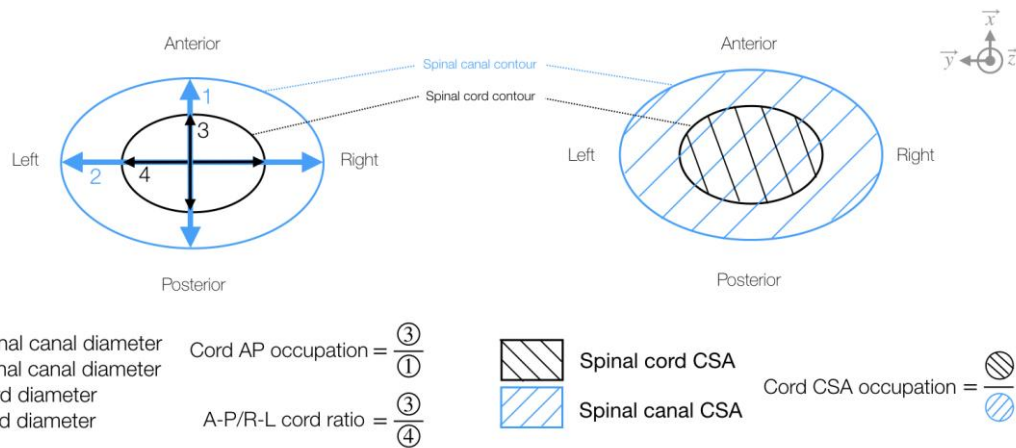


**Figure 1.** Definition of the compression indices measured on anatomical MRI data. Diagrams represent a simplified transversal view of the cord (black outline) and spinal canal (blue outline). A-P: anterior-posterior, R-L: right-left, CSA: Cross-Sectional Area.

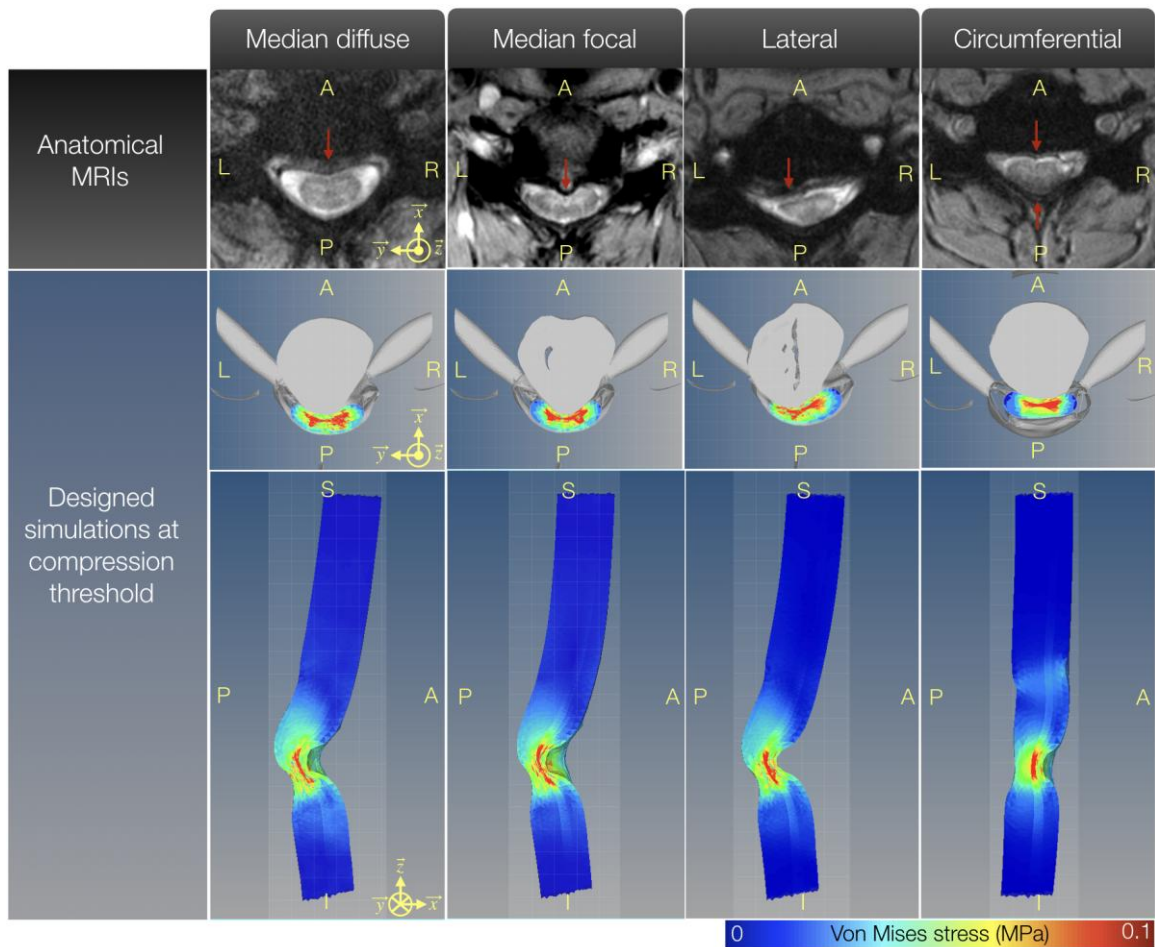


**Figure 2.** Main compression types observed in the DCM group. First row shows anatomical transversal MRIs (T2\*-weighted scans). Red arrows indicate the compression processes occurring as pointed out by the clinician. Second and third rows show the transversal and sagittal views for the corresponding simulations (constraint maps are the Von Mises stress). Anatomical markers are indicated on each image (A: anterior, P: posterior, L: left, R: right).

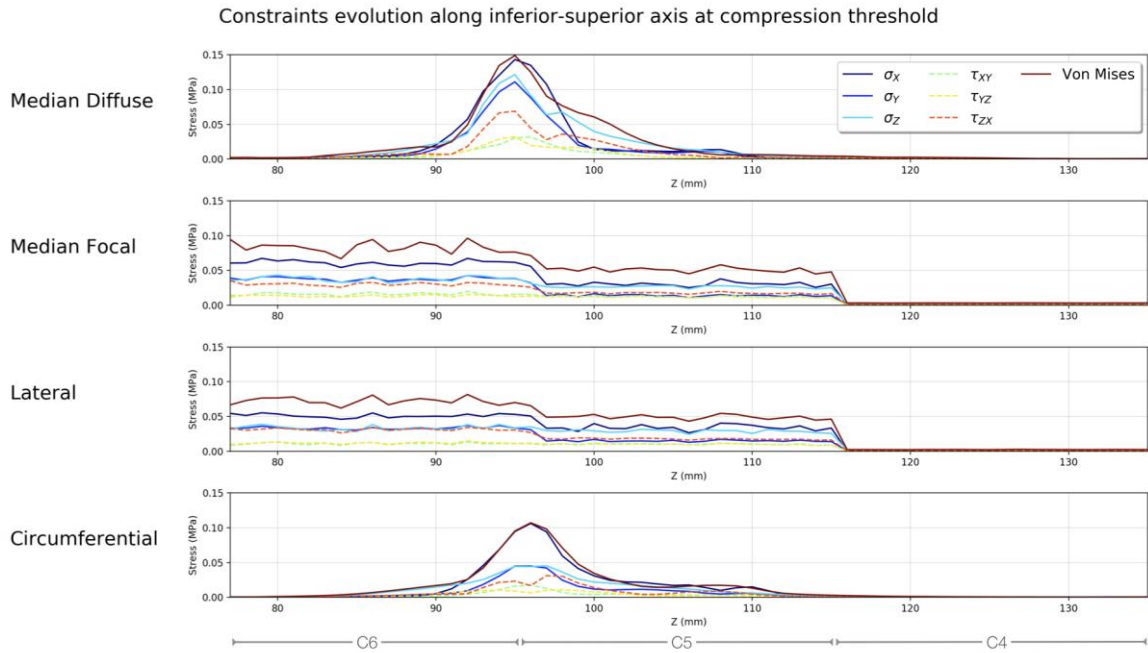


**Figure 3.** Constraints value (95<sup>th</sup> percentile of the absolute value by millimeter) along the inferior-superior axis for each compression type. The extent of each vertebral level is indicated below.  $\sigma_X$ ,  $\sigma_Y$ ,  $\sigma_Z$ : stresses along X, Y, Z;  $\tau_{XY}$ ,  $\tau_{YZ}$ ,  $\tau_{ZX}$ : shear stresses in plane XY, YZ, ZX.

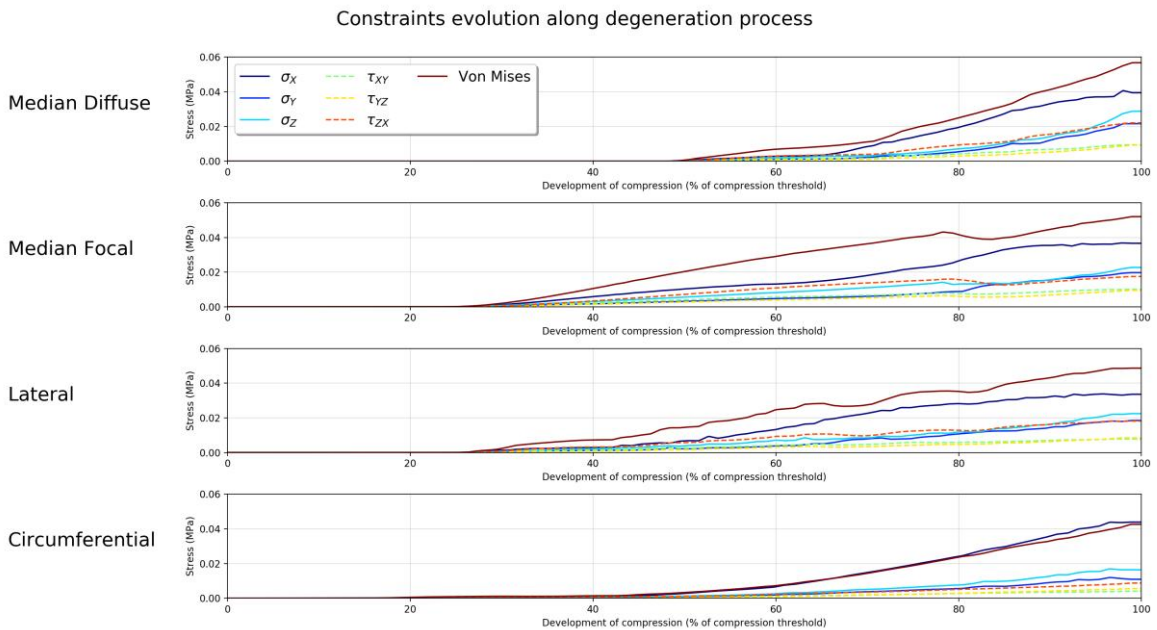
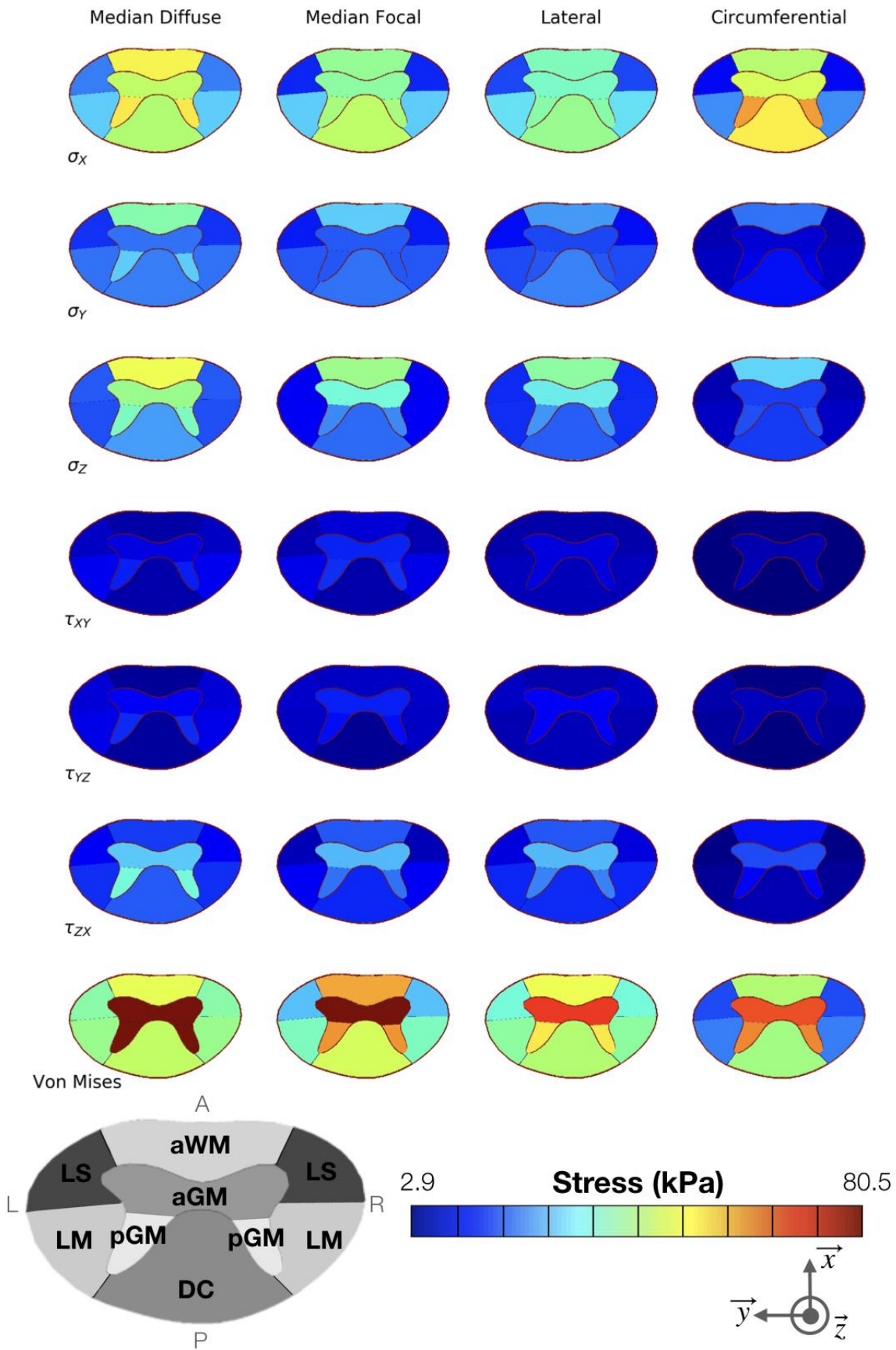


**Figure 4.** Constraints value (95<sup>th</sup> percentile of the absolute value in whole cord at each simulation step) along the development of the compression until threshold, for each type.  $x$ -axis corresponds to the simulation steps until compression threshold is reached. The



1 time sale of degenerative spine changes leading to DCM, which extends over several  
2 years, and the respective timings of individual processes, are unknown. Therefore, care  
3 should be taken when interpreting those results in terms of dynamics.  $\sigma_X$ ,  $\sigma_Y$ ,  $\sigma_Z$ : stresses  
4 along X, Y, Z;  $\tau_{XY}$ ,  $\tau_{YZ}$ ,  $\tau_{ZX}$ : shear stresses in plane XY, YZ, ZX.

5



1  
2

**Figure 5.** Spinal cord regions analysis at compression threshold. Each constraint value (95<sup>th</sup> percentile of the absolute value by region) were quantified and plotted by region on an unwrapped transversal map. Region labels are indicated on the bottom left-hand corner. Note that left and right regions were quantified together to get rid of bias caused by potential asymmetry in compression types (e.g., lateral type). Color scale was defined according to minimum and maximum values across all constraints and regions.  $\sigma_X$ ,  $\sigma_Y$ ,  $\sigma_Z$ : stresses along X, Y, Z;  $\tau_{XY}$ ,  $\tau_{YZ}$ ,  $\tau_{ZX}$ : shear stresses in plane XY, YZ, ZX.

## 7. Acknowledgements

The authors would like to sincerely thank Lauriane Pini, Claire Costes and Véronique Gimenez-Derderian for MR examinations and study logistics as well as Patrice Sudres, Tristan Tarrade and Maxime Llari for useful discussions.

This project has received funding from the European Union's Horizon 2020 research and innovation program under the Marie Skłodowska-Curie grant agreement N°713750. Also, it has been carried out with the financial support of the Regional Council of Provence-Alpes-Côte d'Azur and with the financial support of the A\*MIDEX (n° ANR- 11-IDEX-0001-02), funded by the Investissements d'Avenir project funded by the French Government, managed by the French National Research Agency (ANR).

This work was performed within a laboratory member of France Life Imaging network (grant ANR-11-INBS-0006) and supported by the CNRS (Centre National de la Recherche Scientifique).

## 8. References

1. Nouri A, Tetreault L, Singh A, Karadimas SK, Fehlings MG. Degenerative Cervical Myelopathy: Epidemiology, Genetics, and Pathogenesis. *Spine*. 2015 Jun;40(12):E675–93.
2. Matsumoto M, Fujimura Y, Suzuki N, Nishi Y, Nakamura M, Yabe Y, et al. MRI of cervical intervertebral discs in asymptomatic subjects. *The Journal of Bone and Joint Surgery*. 1998;80(1):6.
3. Ellingson BM, Woodworth DC, Leu K, Salamon N, Holly LT. Spinal Cord Perfusion MR Imaging Implicates Both Ischemia and Hypoxia in the Pathogenesis of Cervical Spondylosis. *World Neurosurgery*. 2019 Aug;128:e773–81.
4. Fehlings MG, Skaf G. A review of the pathophysiology of cervical spondylotic myelopathy with insights for potential novel mechanisms drawn from traumatic spinal cord injury. *Spine*. 1998 Dec 15;23(24):2730–7.
5. Ahuja CS, Wilson JR, Nori S, Kotter MRN, Druschel C, Curt A, et al. Traumatic spinal cord injury. *Nature Reviews Disease Primers*. 2017 Apr 27;3:17018.
6. Nishida N, Kato Y, Imajo Y, Kawano S, Taguchi T. Biomechanical analysis of cervical spondylotic myelopathy: The influence of dynamic factors and morphometry of the spinal cord. *The Journal of Spinal Cord Medicine*. 2012 Jul;35(4):256–61.
7. Kim YH, Khuyagbaatar B, Kim K. Biomechanical effects of spinal cord compression due to ossification of posterior longitudinal ligament and ligamentum flavum: A finite element analysis. *Medical Engineering & Physics*. 2013 Sep;35(9):1266–71.
8. Nishida N, Kanchiku T, Kato Y, Imajo Y, Yoshida Y, Kawano S, et al. Cervical ossification of the posterior longitudinal ligament: Biomechanical analysis of the influence of static and dynamic factors. *The Journal of Spinal Cord Medicine*. 2015 Sep;38(5):593–8.
9. Khuyagbaatar B, Kim K, Park WM, Kim YH. Influence of sagittal and axial types of ossification of posterior longitudinal ligament on mechanical stress in cervical spinal cord: A finite element analysis. *Clinical Biomechanics*. 2015 Dec;30(10):1133–9.
10. Northover JR, Wild JB, Braybrooke J, Blanco J. The epidemiology of cervical spondylotic myelopathy. *Skeletal Radiol*. 2012 Dec 1;41(12):1543–6.
11. Edwards W, LaRocca H. The developmental segmental sagittal diameter of the cervical spinal canal in patients with cervical spondylosis. *Spine*. 1983;8(1):20–7.
12. Penning L. Normal movements of the cervical spine. *American Journal of Roentgenology*. 1978 Feb 1;130(2):317–26.
13. Ogino H, Tada K, Okada K, Yonenobu K, Yamamoto T, Ono K, et al. Canal diameter, anteroposterior compression ratio, and spondylotic myelopathy of the cervical spine. *Spine*. 1983;8(1):1–15.

- 1 14. Arnold JG Jr. The clinical manifestations of spondylochondrosis (spondylosis) of the  
2 cervical spine. *Annals of surgery*. 1955 Jun;141(6):872–89.
- 3 15. Burrows EH. The sagittal diameter of the spinal canal in cervical spondylosis.  
4 *Clinical Radiology*. 1963;14(1):77–86.
- 5 16. Hayashi H, Okada K, Hamada M, Tada K, Ueno R. Etiologic factors of myelopathy.  
6 A radiographic evaluation of the aging changes in the cervical spine. *Clinical*  
7 *orthopaedics and related research*. 1987 Jan;(214):200–9.
- 8 17. Adams CBT, Logue V. Studies in Cervical Spondylotic Myelopathy: II. The  
9 Movement and Contour of the Spine in Relation to the Neural Complications of  
10 Cervical Spondylosis. *Brain*. 1971 Jan 1;94(3):569–86.
- 11 18. Fehlings MG, Rao SC, Tator CH, Skaf G, Arnold P, Benzel E, et al. The optimal  
12 radiologic method for assessing spinal canal compromise and cord compression in  
13 patients with cervical spinal cord injury. Part II: Results of a multicenter study.  
14 *Spine (Phila Pa 1976)*. 1999 Mar 15;24(6):605–13.
- 15 19. Arvin B, Kalsi-Ryan S, Karpova A, Mercier D, Furlan JC, Massicotte EM, et al.  
16 Postoperative Magnetic Resonance Imaging Can Predict Neurological Recovery  
17 After Surgery for Cervical Spondylotic Myelopathy: A Prospective Study With  
18 Blinded Assessments. *Neurosurgery*. 2011 Aug 1;69(2):362–8.
- 19 20. Arvin B, Kalsi-Ryan S, Mercier D, Furlan JC, Massicotte EM, Fehlings MG.  
20 Preoperative Magnetic Resonance Imaging Is Associated With Baseline  
21 Neurological Status and Can Predict Postoperative Recovery in Patients With  
22 Cervical Spondylotic Myelopathy: *Spine*. 2013 Jun;38(14):1170–6.
- 23 21. Nouri A, Tetreault L, Zamorano JJ, Dalzell K, Davis AM, Mikulis D, et al. Role of  
24 Magnetic Resonance Imaging in Predicting Surgical Outcome in Patients With  
25 Cervical Spondylotic Myelopathy: *Spine*. 2015 Feb;40(3):171–8.
- 26 22. Nouri A, Martin AR, Mikulis D, Fehlings MG. Magnetic resonance imaging  
27 assessment of degenerative cervical myelopathy: a review of structural changes and  
28 measurement techniques. *FOC*. 2016 Jun;40(6):E5.
- 29 23. Li X-Y, Lu S-B, Sun X-Y, Kong C, Guo M-C, Sun S-Y, et al. Clinical and magnetic  
30 resonance imaging predictors of the surgical outcomes of patients with cervical  
31 spondylotic myelopathy. *Clinical Neurology and Neurosurgery*. 2018 Nov  
32 1;174:137–43.
- 33 24. Penning L, Wilmink J, van Woerden H, Knol E. CT myelographic findings in  
34 degenerative disorders of the cervical spine: clinical significance. *American Journal*  
35 *of Roentgenology*. 1986 Apr 1;146(4):793–801.
- 36 25. Fujiwara K, Yonenobe S, Hiroshima K, Fuji T, Ebara S, Yamashita K, et al. The  
37 evaluation of viability of the spinal cord by CT myelography. *Rinsho Seikei Geka*.  
38 1986;21(4):355–61.
- 39 26. Nishida N, Kanchiku T, Taguchi T. Biomechanical Analysis of Compressive  
40 Myelopathy: The Influence of Morphometry of the Spinal Cord. In: Uchida K,

- Nakamura M, Ozawa H, Katoh S, Toyama Y, editors. Neuroprotection and Regeneration of the Spinal Cord [Internet]. Tokyo: Springer Japan; 2014. p. 75–82. Available from: [https://doi.org/10.1007/978-4-431-54502-6\\_7](https://doi.org/10.1007/978-4-431-54502-6_7)
27. El-Rich M, Arnoux P-J, Wagnac E, Brunet C, Aubin C-E. Finite element investigation of the loading rate effect on the spinal load-sharing changes under impact conditions. *Journal of Biomechanics*. 2009 Jun 19;42(9):1252–62.
28. Wagnac E, Arnoux P-J, Garo A, Aubin C-E. Finite element analysis of the influence of loading rate on a model of the full lumbar spine under dynamic loading conditions. *Med Biol Eng Comput*. 2012 Sep;50(9):903–15.
29. Ichihara K, Taguchi T, Shimada Y, Sakuramoto I, Kawano S, Kawai S. Gray matter of the bovine cervical spinal cord is mechanically more rigid and fragile than the white matter. *Journal of neurotrauma*. 2001;18(3):361–7.
30. Taso M, Le Troter A, Sdika M, Ranjeva J-P, Guye M, Bernard M, et al. Construction of an in vivo human spinal cord atlas based on high-resolution MR images at cervical and thoracic levels: preliminary results. *MAGMA*. 2014 Jun 1;27:257–67.
31. Standring S. *Gray's Anatomy: The Anatomical Basis of Clinical Practice*, Expert Consult - 40th Edition. 2008.
32. Lévy S, Benhamou M, Naaman C, Rainville P, Callot V, Cohen-Adad J. White matter atlas of the human spinal cord with estimation of partial volume effect. *NeuroImage*. 2015 Spring;119:262–71.
33. Gooding MR, Wilson CB, Hoff JT. Experimental cervical myelopathy: effects of ischemia and compression of the canine cervical spinal cord. *J Neurosurg*. 1975;43:9–17.
34. Shimomura Y, Hukuda S, Mizuno S. Experimental Study of Ischemic Damage to the Cervical Spinal Cord. *Journal of Neurosurgery*. 1968 Jun;28(6):565–81.
35. Ichihara K, Taguchi T, Sakuramoto I, Kawano S, Kawai S. Mechanism of the spinal cord injury and the cervical spondylotic myelopathy: new approach based on the mechanical features of the spinal cord white and gray matter. *Journal of Neurosurgery: Spine* [Internet]. 2003;99(3). Available from: <https://thejns.org/spine/view/journals/j-neurosurg-spine/99/3/article-p278.xml>
36. Koser DE, Moeendarbary E, Hanne J, Kuerten S, Franze K. CNS Cell Distribution and Axon Orientation Determine Local Spinal Cord Mechanical Properties. *Biophysical Journal*. 2015 May;108(9):2137–47.
37. Ozawa H, Matsumoto T, Ohashi T, Sato M, Kokubun S. Comparison of spinal cord gray matter and white matter softness: measurement by pipette aspiration method. *Journal of Neurosurgery: Spine*. 2001 Oct;95(2):221–4.
38. Alshareef M, Krishna V, Ferdous J, Alshareef A, Kindy M, Kolachalama VB, et al. Effect of Spinal Cord Compression on Local Vascular Blood Flow and Perfusion Capacity. *PloS one*. 2014;9:e108820.

